THE ASTROPHYSICAL JOURNAL, 401:574–583, 1992 December 20

THE LOW FILLING FACTOR OF DUST IN THE GALAXY

JAYANT MURTHY,[1] H. J. WALKER,[2,3] AND R. C. HENRY[1]
Received 1992 March 4; accepted 1992 June 23

ABSTRACT

We have examined the neighborhood of 745 luminous stars in the *IRAS* Skyflux plates for the presence of dust heated by the nearby star. This dust may be distinguished from the ubiquitous cool cirrus by its higher temperature and thus enhanced 60 μm emission. We have found 123 dust clouds around only 106 of the stars with a volume filling factor of 0.006 and an intercloud separation of 46 pc. Nowhere do we find a region where the dust is smoothly distributed through the volume of space heated by the star and hence we place an upper limit of 0.05 cm^{-3} on the equivalent gas density in the intercloud regions. From the lack of infrared emission near the star, we find that less than 1% of the stellar luminosity is reprocessed within 10 pc of the star.

The clouds, themselves, have an average density of 0.22 cm^{-3} (assuming a standard gas-to-dust ratio) and a radius of 1.9 pc, albeit with wide variations in their properties. We have tentatively identified these clouds with the warm, ionized medium of McKee & Ostriker. We have found two different scale heights of 140 and 540 pc for the number of clouds around different groups of stars which we have interpreted as evidence for different distributions of dust in and out of the Galactic disk. The dust at higher altitudes also appears to be more uniformly distributed with Galactic latitude.

Subject headings: dust, extinction — ISM: general — reflection nebulae

1. INTRODUCTION

One of the major achievements of the *Infrared Astronomical Satellite* (*IRAS*) was its survey of 96% of the sky in four wavelength bands centered at 12, 25, 60, and 100 μm (for details see the *IRAS* Explanatory Supplement 1986). By far the most dominant component seen at 100 μm is emission from the cirrus (Low et al. 1984), dust that is heated by the interstellar radiation field (ISRF); detailed surveys of the dust in our Galaxy, similar to the H I surveys (e.g., Heiles 1975), can be made (see, for example, Boulanger & Perault 1988).

In this work, we have used the *IRAS* Skyflux plates to study the environment in the vicinity of 745 luminous stars. Dust near these stars will be heated by the stellar radiation field to higher temperatures than the cool cirrus, from which it may be distinguished by an enhanced 61/100 μm flux density ratio. Conversely, if there is no emission near these stars, or only emission from the cool cirrus along the line of sight, we may place limits on the amount of dust and, by extension, on the amount of matter near those stars. As the distances to the stars in our program are known (or can be estimated), the dust distribution around those stars provides a probe of the three-dimensional structure of the interstellar medium (ISM) in our Galaxy.

We have found dust clouds around 106 of the 745 stars in our survey for a number fraction of 0.14 ± 0.05, slightly less than, but still consistent with, the value of 0.2 ± 0.11 found by Van Buren (1989) for a smaller sample of stars near the Galactic plane. However, many of these clouds occupy only a small fraction of the total volume around each star, implying a much lower volume filling factor. We will reserve discussion of the individual clouds for a future paper, here discussing only the environment of the stars and its implications for the global morphology of the dust.

2. DATA ANALYSIS

As mentioned above, we have examined the *IRAS* Skyflux plates, which are binned in 2′ pixels with an effective resolution of 6′ at all four wavelengths, in the neighborhood of 745 stars, selected primarily from the Bright Star Catalog (Hoffleit 1982). All of the O and B stars in the Bright Star Catalog have been selected and, in addition, all stars of luminosity class I were also examined. Finally, we added all the O stars in the SKYMAP data base (Gottlieb 1978). Several regions (Table 1) were excluded from our analysis, including regions within 10° of the Galactic plane, where background subtraction become problematic, and several regions of known molecular cloud concentrations, such as Orion or Taurus. (These regions are identical to those excluded by Boulanger & Perault 1988.) The distribution of our target stars in galactic coordinates is shown in Figure 1. The spectral type, apparent magnitude, and observed $B-V$ for each star were obtained from the Bright Star Catalog; the absolute magnitude, temperaure, and intrinsic $B-V$ were read from tables in Zombeck (1982); and the $E(B-V)$, spectroscopic distance, and luminosity of the star were calculated from the other quantities.

Although virtually all of the emission in the *IRAS* Skyflux plates is due to dust (interplanetary, circumstellar, or interstellar), we are interested in only that part which is actually due to dust heated by the star in question. The remainder, consisting primarily of zodiacal light and the cool cirrus, must therefore be identified and subtracted. We attempted to develop an automated computer procedure to do this but found that, in practice, we were limited to removing only the smooth component of the background, leaving behind any discrete structures, whether associated with the star or not. The first step in our procedure was to select a region of typically 6.°7 × 6.°7 (201 × 201 pixels) centered on the star (this region

[1] Department of Physics and Astronomy, Johns Hopkins University, Baltimore, MD 21218.
[2] SETI Institute, 2035 Landings Drive, Mountain View, CA 94043.
[3] Rutherford Appleton Laboratory, Chilton, Didcot, Oxon, UK.

TABLE 1

REGIONS EXCLUDED IN OUR SURVEY

Name	Galactic Longitude	Galactic Latitude
Carina	$245 < l < 275$	$-20 < b < -10$
Cepheus	$98 < l < 141$	$10 < b < 22$
Chamaeleon	$290 < l < 305$	$-20 < b < -10$
Galactic plane	$0 < l < 360$	$-10 < b < 10$
LMC	$273 < l < 286$	$-38 < b < -30$
Lupus	$315 < l < 360$	$10 < b < 30$
Ophiuchus	$l < 50$	$10 < b < 20$
Orion	$190 < l < 220$	$-22.5 < b < -10$
Perseus	$150 < l < 170$	$-32.5 < b < -10$

was smaller if the star was near the edge of a plate) and divide it into blocks of 20 × 20 pixels. We then fitted a grid consisting of the minimum values in each of the blocks by a quadratic surface, which formed our estimate of the smooth background contribution to the plate. In order to ensure that the background was not affected by large bright clouds completely filling a block, we rejected any pixels with intensities more than 3 σ over the mean (of all the pixels) and repeated the procedure. An example of our fit is shown in Figure 2. We obtained an estimate of the quality of our fits from the rms deviations in a relatively flux-free region of each plate. The average deviations for our entire sample are 0.14, 0.20, 0.15, and 0.31 MJy sr^{-1} in the 12, 25, 60, and 100 μm bands, respectively, and are on the same order as errors cited by other groups using similar procedures (e.g., Boulanger et al. 1990).

The remaining emission in the plate consists of not only dust clouds heated by the star but also cool cirrus clouds only coincidentally in the same direction as the star, and we must differentiate between the two. Our selection criteria were that the cloud exist as a distinct entity in the 60 μm map (not necessarily centered on the star) and that the 60/100 μm ratio within the cloud increase toward the star. We have found 123 such clouds (Table 2) around 106 stars, ranging in size and brightness from the large, bright (and well-known) clouds around ζ Oph (HD 149757; Van Buren & McCray 1988) and

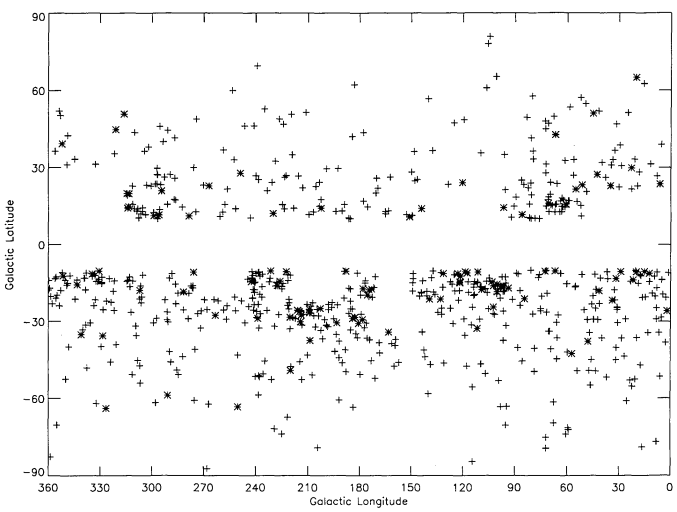

FIG. 1.—The distribution of the stars in our program in Galactic coordinates is shown. Those stars around which we have found dust clouds are plotted as asterisks. Note that we have excluded several regions from consideration, including the Galactic plane, Orion, and Taurus, among others (see Table 1).

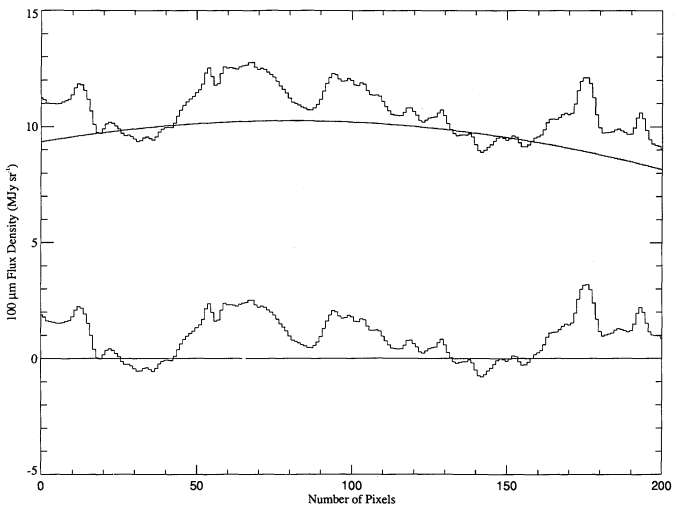

FIG. 2.—A cut through the original Skyflux plate is shown (*upper line*) with our fit to the background emission (*smooth line*). The lower line shows the residual emission. Some of the overall curvature in the original plate has been removed, without affecting the discrete features.

α Cam (HD 30614; de Vries 1985) to those barely distinguishable from the background. In order to estimate the errors in this procedure, we have performed our search twice, with different people, finding agreement in 638 out of the 745 total cases, or in 86% of the cases. This difference is, however, proportionately greater in the number of clouds as 123 clouds were found the first time and 144 the second, with agreement in 67 cases. Not only is there ambiguity in deciding whether a faint path is due to emission from dust heated by the star but there are a significant number of bright features for which it was a subjective decision whether there was an increase in the 60/100 μm ratio toward the star or not. Nevertheless, despite these problems, it is clear that most of the stars in our survey do not have detectable dust clouds nearby.

Selection effects are important in our data and two of them are illustrated in Figure 3, where we have plotted the radius of the clouds as a function of distance from the Sun. The first of these biases is introduced through a finite spatial resolution of the instrument: distant clouds must be larger in order to be above the resolution limit (solid line in Fig. 3). In addition to small clouds not being detected at large distances, the converse effect is also present. This is primarily due to our selection by apparent magnitude: the nearer stars tends to be less intrinsically luminous and thus will not illuminate a large cloud in its entirety. That this is a factor in our results is shown in Figure 4 where we have expressed the radius of the cloud as a fraction of the distance at which the stellar radiation field drops to the level of the ISRF. It should be noticed that the nearby clouds are not significantly smaller, in relation to the stellar luminosity, than those at greater distances. Another consequence of our selection by magnitude is that we automatically discriminate against stars in high obscuration regions where there are more likely to be dust clouds. Finally, as the more luminous stars will both dominate over the ISRF for a larger volume of space and heat dust within that volume to higher temperature, we will be more likely to detect clouds around those stars (Table 3). As a corollary, we will be more likely to observe dust clouds around more distant stars, which tend to be intrinsically brighter, but the clouds will be larger, due to the instrumental resolution.

TABLE 2

STARS WITH DUST CLOUDS

Number (1)	HD (2)	Spectral Type (3)	l (4)	b (5)	V (6)	Distance (pc) (7)	r_c (pc) (8)	d_c (pc) (9)	Density (cm^{-3}) (10)	F_{12} (11)	F_{25} ($\times 10^{-5}$ ergs s^{-1}) (12)	F_{60} ($\times 10^{-5}$ ergs s^{-1}) (13)	F_{100} ($\times 10^{-5}$ ergs s^{-1}) (14)
1	358	B81 IV	111.7	−32.8	2.1	58	0.1	0.3	8.52	35.3	22.2	3.7	2.5
2	1337	O9 III	117.6	−11.1	6.1	1719	4.5	11.6	1.00	9.1	4.5	3.8	4.9
3	1976	B5 IV	118.7	−10.6	5.6	283	1.7	0.8	1.47	5.1	4.5	4.3	4.9
4	3901	B2 V	121.4	−12.3	4.8	530	1.8	1.6	0.62	7.5	6.0	12.4	6.5
5	4142	B5 V	121.7	−15.0	5.7	215	0.6	0.3	1.70	2.2	2.4	3.3	2.3
6	4180	B5 III	121.8	−14.6	4.5	216	0.7	0.9	2.11	6.4	2.4	2.9	2.8
7	4180	B5 III	121.8	−14.6	4.5	216	0.8	1.0	1.86	6.6	1.3	3.3	3.5
8	4881	B9 V	123.0	−11.3	6.2	108	0.4	0.2	5.48	7.7	4.2	5.0	4.3
9	10144	B3 V	290.8	−58.8	0.5	80	0.2	1.8	3.61	26.2	4.6	1.7	1.3
10	10205	B8 III	132.9	−21.3	4.9	281	0.6	0.3	0.29	3.8	4.8	1.4	0.7
11	10516	B2 V	131.3	−11.3	4.1	341	0.8	3.4	3.37	7.9	4.5	4.0	4.1
12	10516	B2 V	131.3	−11.3	4.1	341	0.9	4.5	5.28	17.7	6.5	4.1	5.5
13	10516	B2 V	131.3	−11.3	4.1	341	0.5	2.7	2.63	23.9	11.3	2.3	1.9
14	13294	B9 V	139.4	−21.3	5.6	85	0.1	0.2	5.48	13.9	7.2	1.5	1.3
15	17098	B9 V	250.3	−63.3	6.4	119	0.2	0.2	1.66	3.9	3.9	1.4	0.8
16	19374	B1 V	163.0	−34.2	6.1	967	3.6	3.5	0.41	10.9	13.3	3.7	3.5
17	24587	B6 V	220.0	−49.1	4.7	138	0.2	0.2	1.67	3.7	1.9	4.0	1.5
18	25204	B3 V	178.4	−29.4	3.5	302	0.9	3.2	7.64	7.4	3.1	5.0	6.6
19	25204	B3 V	178.4	−29.4	3.5	302	0.9	2.5	2.51	10.1	8.3	3.5	3.7
20	25204	B3 V	178.4	−29.4	3.5	302	0.6	1.8	1.76	5.7	2.0	3.0	2.2
21	25330	B5 V	180.8	−30.8	5.7	175	0.6	1.0	20.1	3.0	1.6	2.7	5.2
22	25330	B5 V	180.8	−30.8	5.7	175	0.5	0.7	4.99	9.0	3.1	2.4	3.1
23	26676	B8 V	182.7	−28.4	6.2	227	0.7	0.3	11.1	15.3	11.1	26.0	19.6
24	26912	B3 IV	184.2	−28.9	4.3	532	5.2	3.4	0.88	6.6	2.3	8.8	9.4
25	27742	B8 IV	175.3	−19.7	6.0	290	0.9	0.6	2.78	80.2	7.5	2.5	2.9
26	27778	B3 V	172.8	−17.4	6.4	746	2.4	4.0	6.66	5.0	5.3	4.6	7.6
27	28149	B7 V	174.3	−17.7	5.5	202	1.0	0.4	7.07	17.3	6.7	18.6	16.7
28	28375	B3 V	193.4	−30.6	5.6	765	2.2	1.8	0.52	7.4	4.9	4.6	3.5
29	29365	B8 V	177.9	−17.2	5.9	229	0.7	0.7	29.2	−6.9	5.7	4.0	8.1
30	30614	O9 Ia	144.1	14.0	4.3	966	16.7	7.0	0.07	5.9	6.2	9.9	5.7
31	32343	B2 V	151.0	10.8	5.1	577	2.7	3.8	2.51	14.1	5.0	6.4	7.2
32	32343	B2 V	151.0	10.8	5.1	577	1.4	5.4	5.58	8.0	3.1	3.2	5.0
33	32612	B2 IV	214.3	−30.2	6.4	1626	3.3	5.3	1.16	0.1	4.4	2.9	3.5
34	33328	B2 IV	209.1	−26.7	4.3	616	4.8	2.9	0.12	8.8	1.9	3.8	2.6
35	32686	B5 IV	203.0	−25.0	6.1	348	1.3	1.0	8.01	15.8	3.8	8.8	12.8
36	33949	B9 V	213.9	−27.5	4.4	53	0.2	0.2	10.4	4.7	−1.4	3.2	3.3
37	34085	B8 Ia	209.2	−25.2	0.1	222	1.1	5.1	1.48	11.4	6.5	4.3	4.2
38	34085	B8 Ia	209.2	−25.2	0.1	222	1.0	2.3	0.28	7.2	0.8	4.1	2.0
39	34085	B8 Ia	209.2	−25.2	0.1	222	1.2	5.7	1.57	9.2	8.1	4.4	4.8
40	34085	B8 Ia	209.2	−25.2	0.1	222	0.7	7.0	5.96	12.2	8.0	3.9	5.2
41	34085	B8 Ia	209.2	−25.2	0.1	222	1.0	6.6	2.73	10.9	3.6	3.3	4.1
42	34085	B8 Ia	209.2	−25.2	0.1	222	0.8	7.1	23.8	43.6	16.0	15.0	20.1
43	34798	B3 V	220.3	−28.4	6.4	1214	2.1	2.7	0.65	1.7	0.5	1.1	1.3
44	34816	B0 IV	214.8	−26.2	4.3	649	1.3	10.1	4.68	9.5	6.3	2.1	3.4
45	35337	B2 IV	216.0	−25.7	5.2	996	2.9	7.8	2.55	5.9	3.1	2.2	3.8
46	35532	B2 Vn	188.0	−10.3	6.2	989	5.7	2.9	0.25	7.9	3.9	4.1	3.6
47	37795	B7 IV	238.8	−28.9	2.6	76	0.1	0.3	1.94	5.5	1.3	1.5	0.9
48	42933	B3 III	263.3	−27.7	4.8	998	5.2	2.0	0.08	3.8	3.0	3.7	2.2
49	43955	B2 V	227.5	−16.1	5.5	818	1.7	4.3	1.44	3.9	1.0	1.4	1.8
50	44743	B1 II	226.1	−14.3	2.0	308	3.7	7.1	0.44	6.9	4.0	3.6	3.7
51	46064	B1 V	222.4	−10.5	6.2	1034	3.3	3.4	0.42	4.6	2.7	2.8	2.5
52	49333	B7 III	231.4	−10.3	6.1	541	1.6	0.8	1.33	13.9	3.7	3.1	3.3
53	50013	B1 IV	242.4	−14.5	4.0	557	1.3	9.6	9.03	5.7	5.0	2.5	4.8
54	58050	B2 V	202.5	14.2	6.4	1233	3.4	5.5	1.01	4.2	7.7	1.5	2.4
55	67159	B9 V	230.0	12.1	6.2	121	0.2	0.2	17.9	2.7	2.8	1.4	2.0
56	68520	B6 IV	281.6	−18.6	4.3	161	0.3	0.6	7.10	6.4	2.7	2.8	2.9
57	74375	B1 II	275.8	−10.9	4.3	635	8.8	7.6	0.29	6.4	2.7	3.4	4.5
58	83754	B5 V	248.7	27.8	5.1	169	0.5	0.4	0.68	4.9	2.4	1.6	1.2
59	83754	B5 V	248.7	27.8	5.1	169	0.5	0.5	1.44	2.9	2.3	1.4	1.3
60	89353	B9 Ib	266.8	22.9	5.3	806	1.4	1.2	0.18	92.7	8.7	1.3	0.8
61	91355	B9	278.6	11.1	5.7	108	0.2	0.2	28.9	5.7	0.5	2.6	4.1
62	91356	B4	278.6	11.1	6.1	215	0.3	0.9	26.0	5.5	0.8	2.7	4.3
63	105383	B9 V	296.0	11.5	6.4	125	0.5	0.2	3.57	19.0	11.3	8.0	5.8
64	105521	B3 IV	294.4	20.9	5.5	935	1.9	4.3	3.15	4.9	2.4	3.5	4.7
65	105521	B3 IV	294.4	20.9	5.5	935	2.4	2.3	0.47	7.1	4.2	4.0	3.0
66	108257	B3 V	299.0	11.2	4.8	580	4.8	2.5	0.87	4.0	2.5	6.1	6.5
67	116658	B1 III	316.1	50.8	1.0	162	0.8	1.9	0.25	8.6	8.8	5.8	2.3
68	119361	B8 III	313.2	19.8	6.0	447	1.2	0.9	1.78	6.4	4.5	1.6	2.2
69	119605	G0 Ib	321.0	44.8	5.6	816	1.4	0.8	0.92	3.2	3.6	1.4	1.5

TABLE 2—*Continued*

Number (1)	HD (2)	Spectral Type (3)	l (4)	b (5)	V (6)	Distance (pc) (7)	r_c (pc) (8)	d_c (pc) (9)	Density (cm^{-3}) (10)	F_{12} (11)	F_{25} ($\times 10^{-5}$ ergs s^{-1}) (12)	F_{60} ($\times 10^{-5}$ ergs s^{-1}) (13)	F_{100} ($\times 10^{-5}$ ergs s^{-1}) (14)
70.....	120307	B2 IV	314.4	19.9	3.4	433	0.9	3.6	0.97	4.4	2.7	2.5	2.0
71.....	120307	B2 IV	314.4	19.9	3.4	433	1.1	3.0	0.40	4.4	1.9	2.7	1.9
72.....	120640	B2 V	313.5	14.7	5.8	892	2.9	4.7	1.50	7.1	4.3	3.4	4.7
73.....	121263	B2 IV	314.1	14.2	2.5	291	1.1	5.3	2.97	11.8	6.8	4.3	5.0
74.....	124771	B4 V	306.9	−18.0	5.1	155	0.8	0.4	3.75	3.1	4.3	9.5	7.2
75.....	128220	O7 III	20.1	64.9	8.5	3158	8.2	7.1	0.06	5.6	3.8	1.7	1.3
76.....	135742	B8 V	352.0	39.2	2.6	54	0.1	0.2	3.96	12.9	6.5	2.3	1.5
77.....	141527	G0 I	45.1	51.0	5.8	3526	8.1	1.6	0.06	66.3	10.0	1.9	1.2
78.....	149630	B9 V	66.9	42.7	4.2	43	0.0	0.2	5.93	6.3	2.7	0.9	0.5
79.....	149757	O9 V	6.3	23.6	2.6	168	1.0	7.9	10.8	19.4	14.6	15.3	20.7
80.....	151525	B9	22.9	29.8	5.2	71	0.1	0.2	20.8	5.9	34.9	1.8	2.3
81.....	153261	B2 IV	330.7	−10.3	6.1	1135	2.0	5.4	2.47	8.8	4.4	3.2	3.9
82.....	157246	B1 I	334.6	−11.5	3.3	688	3.0	9.8	0.91	7.8	7.9	6.1	6.4
83.....	157246	B1 I	334.6	−11.5	3.3	688	3.6	13.1	1.70	10.7	6.3	6.5	9.0
84.....	158148	B5 V	42.7	27.3	5.5	205	0.4	0.7	7.25	21.7	14.8	1.1	1.5
85.....	159082	B9 V	35.0	22.9	6.4	121	0.3	0.2	10.6	6.3	2.4	2.5	3.0
86.....	163506	F2 Ib	51.4	23.2	5.5	1111	3.5	0.3	0.14	114.5	35.8	4.8	2.1
87.....	166014	B9 V	55.2	21.6	3.8	37	0.0	0.2	10.4	3.3	3.5	1.3	1.0
88.....	167257	B9 V	343.1	−15.7	6.1	110	0.2	0.2	4.92	7.5	5.9	2.0	1.8
89.....	167756	B0 Ia	351.5	−12.3	6.3	3301	10.5	15.4	0.27	9.5	7.7	5.8	5.9
90.....	172958	B8 V	60.8	15.7	6.4	282	0.5	0.3	2.96	−1.3	−0.2	1.8	1.7
91.....	175360	B8	12.5	−11.3	5.9	220	0.8	0.2	0.95	34.8	18.8	5.0	3.4
92.....	175876	O6	15.3	−10.6	6.9	2741	9.6	5.3	0.08	75.5	43.4	10.2	5.3
93.....	176502	B3 V	70.9	16.0	6.2	1138	3.0	3.3	1.14	2.3	1.1	2.2	3.0
94.....	177817	B8 IV	20.0	−10.7	6.0	327	0.8	0.4	1.82	19.0	15.5	5.0	4.1
95.....	181615	B2 V	21.8	−13.8	4.6	356	0.7	1.7	1.41	174.7	31.6	5.1	2.7
96.....	181858	B3 IV	29.1	−10.6	6.7	1524	2.8	1.9	0.17	6.5	5.4	2.7	1.7
97.....	184915	B0 II	31.8	−13.3	4.9	689	1.4	7.5	2.41	8.5	10.5	3.5	3.8
98.....	186042	B8	2.1	−25.9	6.2	234	0.5	0.5	8.11	1.5	0.0	2.4	3.5
99.....	189775	B5 III	86.0	11.5	6.2	541	0.9	0.9	3.55	106.1	16.7	3.6	3.5
100.....	191639	B1 V	34.0	−21.7	6.5	1204	2.9	2.6	0.20	7.1	8.6	2.7	1.9
101.....	191692	B9 II	41.6	−18.1	3.2	46	0.2	0.4	48.3	12.8	11.7	3.9	6.7
102.....	193924	B2 IV	340.9	−35.2	1.9	213	0.4	3.9	3.19	9.3	7.1	2.6	2.3
103.....	193964	B9 V	96.5	14.4	5.7	92	0.2	0.2	5.10	3.7	0.5	1.7	1.4
104.....	196519	B9 III	328.4	−35.6	5.2	109	0.2	0.2	4.67	3.0	3.2	2.0	1.9
105.....	196740	B5 IV	67.0	−10.3	5.0	228	0.7	0.7	2.41	4.1	2.5	3.0	3.1
106.....	199140	B2 IIIv	72.8	−10.5	6.6	1858	4.3	2.0	0.07	4.0	1.8	4.0	1.8
107.....	204867	G0 Ib	48.0	−37.9	2.9	229	0.5	0.8	2.04	4.2	5.4	1.7	1.8
108.....	209409	B7 IV	57.4	−42.7	4.7	178	0.5	0.5	1.77	6.0	6.1	2.7	2.3
109.....	209833	B9 V	84.5	−21.3	5.6	89	0.2	0.2	16.3	2.9	1.8	2.0	2.8
110.....	212710	B9 V	120.2	24.1	5.3	73	0.1	0.3	76.3	1.8	2.4	0.8	1.7
111.....	212883	B2 V	93.6	−17.0	6.5	1172	3.1	1.0	0.5	4.1	7.5	3.5	1.3
112.....	214168	B2 V	96.4	−16.1	5.7	863	4.1	3.2	0.44	5.0	2.5	4.4	4.2
113.....	214680	O9 V	96.7	−17.0	4.9	769	2.7	6.2	0.49	8.9	4.0	4.0	3.6
114.....	214680	O9 V	96.7	−17.0	4.9	769	1.7	6.3	1.09	5.1	4.6	3.8	3.5
115.....	214993	B2 III	97.7	−16.2	5.2	1031	3.6	3.9	0.24	9.8	4.7	4.1	3.2
116.....	216200	B3 IV	100.0	−15.5	5.9	917	1.9	4.7	2.46	2.5	2.0	1.7	2.5
117.....	217101	B2 IV	100.1	−18.5	6.2	1399	4.5	3.9	0.44	8.2	3.7	5.3	4.7
118.....	217675	B6 III	102.2	−16.1	3.6	148	1.0	0.6	1.83	7.2	3.4	9.0	6.4
119.....	217811	B2 V	103.1	−14.6	6.4	937	2.8	3.1	0.51	3.8	5.5	2.8	2.6
120.....	219927	B8 III	102.3	−24.4	6.3	523	1.2	0.6	0.93	5.8	4.9	2.7	2.3
121.....	222173	B8 V	109.0	−17.6	4.3	116	0.3	0.3	2.79	4.9	4.5	1.6	1.5
122.....	222304	B9 V	111.3	−10.8	5.3	77	0.2	0.2	13.49	4.7	1.6	1.2	1.7
123.....	223145	B3 V	326.6	−63.9	5.2	737	1.5	1.9	0.30	4.9	1.9	1.4	1.1

NOTES.—Col. (7) is the spectroscopic distance of the star from the Sun. Cols. (8) and (9) are, respectively, the distance of the cloud from the star, as defined by the average 60/100 μm ratio in the cloud (see text), and the average radius of the cloud, assuming a spherical cloud. Col. (10) is the average density in the cloud using the 100 μm flux density. Cols. (11) through (14) are, respectively, the average 12, 25, 60, and 100 μm flux densities of the cloud.

In order to model the emission from the dust near the star, or to place upper limits on the amount present, we simply set equal the heat input from the star into the dust, calculated using a Kurucz model (Kurucz 1979) of the appropriate temperature multiplied by a dust absorption profile from Draine & Lee (1984), and the radiation emitted by the dust as a function of the dust temperature, again using optical constants from Draine & Lee. The predicted signal in each of the *IRAS* bands was found by convolving the calculated dust emission profile with the instrument response function. In Figure 5, we have plotted the expected emission at 100 μm from stars of several spectral types placed in a uniformly distributed medium of density 0.1 cm^{-3} as a function of distance from the star. (The density of the dust is quoted here, and elsewhere in this work, in terms of the equivalent amount of H I, assuming the canonical gas to dust ratio of 5.8×10^{21} atoms cm^{-3} mag^{-1}; Bohlin, Savage, & Drake 1978. Note that this is implicit in the Draine & Lee model.)

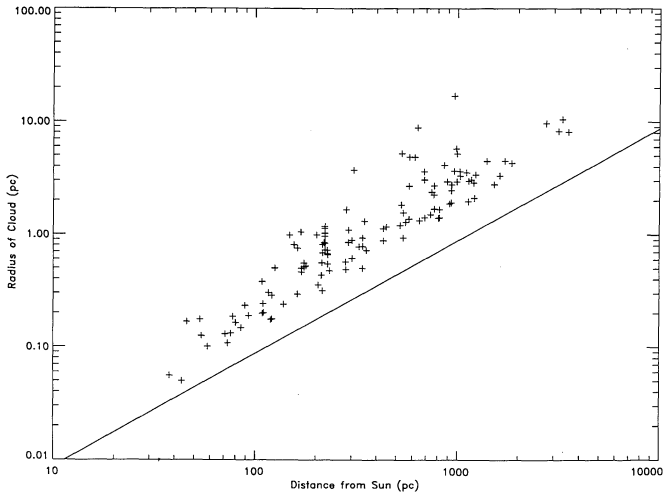

FIG. 3.—The radius of each of our clouds is plotted as a function of distance from the Sun. Clouds which fell below the solid line cannot be detected in our survey because of the finite spatial resolution of the instrument. In addition, large clouds near the Sun are not detected because the nearby stars are, in general, too intrinsically faint to illuminate large clouds in their entirety.

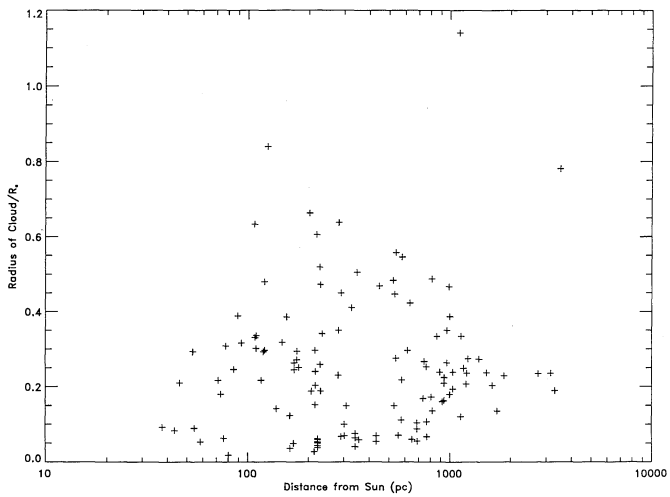

FIG. 4.—The radius of the cloud divided by the distance at which the stellar heating drops to the level of the ISRF (R_s) is plotted against distance from the Sun. From this plot, we see that the tendency for the nearby detected clouds to be smaller is probably due to the lower luminosities of the closer stars and thus is an observational artifact.

3. RESULTS AND DISCUSSION

3.1. *Cloud Properties*

In the present work, we are concerned only with the group properties of the cloud listed in Table 2 and so have used several approximations to characterize them. We have assumed spherical clouds with a radius given by the average length over two orthogonal axes (defined by the plate in question) at a distance from the exciting star such that the predicted 60/100 μm ratio is equal to the observed value (defined as the average over the entire cloud). The amount of dust in each cloud was estimated by calculating an emissivity per grain based on the ratio of the 60/100 μm emission in each pixel, dividing into the observed emission in that pixel, and summing over all the pixels in the cloud. Finally, the average density in the cloud was obtained by dividing by the volume.

We have tabulated the average properties of the detected clouds in Table 4. We find an average cloud radius of 1.9 pc and an average (equivalent H I) density of 0.2 cm^{-3}. However, there is a wide variation in cloud sizes and most have a radius of less than 0.5 pc and a density of less than 0.05 cm^{-3}, as may be seen from the histograms in Figures 6 and 7. The column density through one of these clouds is typically less than about 10^{19} cm^{-2}. Their properties are strongly reminiscent of the warm clouds (warm, ionized medium) in the McKee & Ostriker (1977) theory, of which one example may be the local cloud around our Sun (Bruhweiler & Vidal-Madjar 1987).

We can calculate an average intercloud distance by noting that the total volume of space probed in our program is

TABLE 4

CLOUD PROPERTIES

Parameter	Value
Total number of clouds	123
Total volume of clouds	4.3×10^4 pc^3
Total number of atoms	2.8×10^{59} atoms
Average density	0.22 cm^{-3}
Total volume probed	6.3×10^6 pc^3
Total radiation emitted by clouds	3.7×10^{36} ergs s^{-1}
Total stellar radiation	4.0×10^{40} ergs s^{-1}
Average cloud radius	1.9 pc
Average cloud distance from star	2.8 pc

6.3×10^6 pc^3, where the volume probed by a star is defined to be that region in which the stellar radiation field exceeds the interstellar value. As we detect 123 clouds in this volume, this implies that there is one cloud per 5.1×10^4 pc^3 or that there is an average of 46 pc between clouds. This is much larger than the intercloud distance of 12 pc (for the warm, ionized clouds) in McKee & Ostriker (1977). The total volume of space occupied by our clouds if 4×10^4 pc^3 leading to a filling factor of 0.006, much lower than the 0.23 in the McKee-Ostriker theory.

This is a very low filling factor, and it is important that we understand both what we are measuring and the uncertainties in our procedure. Unfortunately, because of our observational biases, we do not sample a complete cloud distributed at any point and it is difficult for us to estimate by how much we

TABLE 3

STELLAR LUMINOSITY EFFECTS

Parameter	$L_* < 10^{37}$ ergs s^{-1}	$L_* > 10^{37}$ ergs s^{-1}
Number of stars	550	195
Number of stars heating dust	52	54
Number of clouds	55	68
Fraction of stars heating dust	0.09	0.28
Average number of clouds per star	1.06	1.26
Average cloud radius (pc)	0.59	2.99

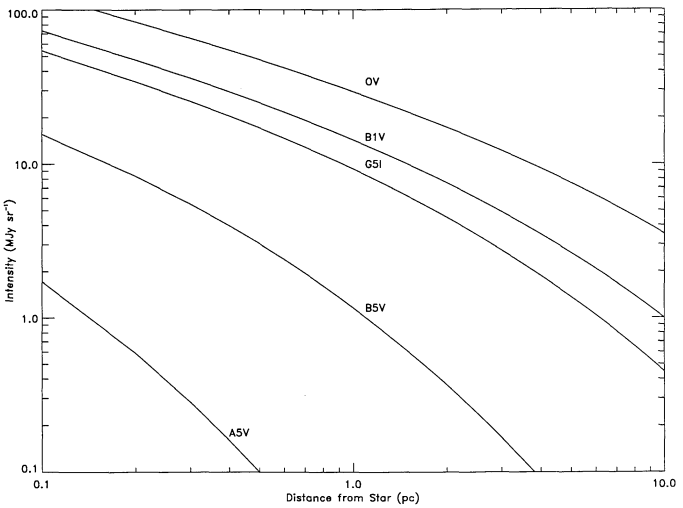

FIG. 5.—The emission seen from the dust at the given distance from the star is plotted for several different spectral types, assuming a uniform dust distribution of density 0.1 cm^{-3}. The radiation field from a hot star may light up dust clouds for many parsecs around.

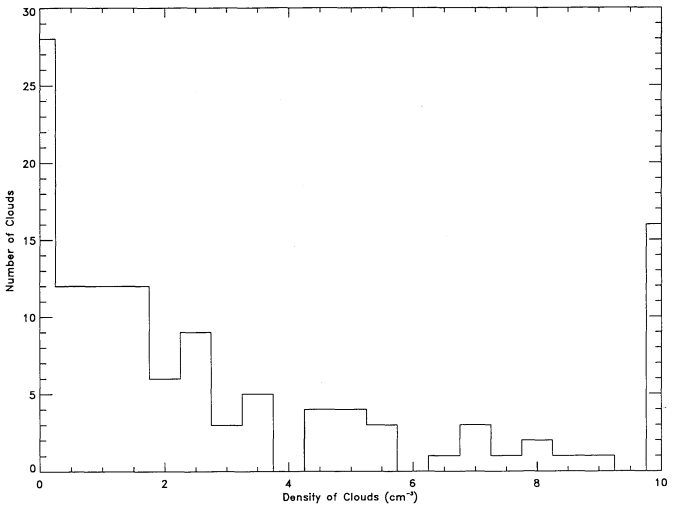

FIG. 7.—A histogram of the density of the clouds is plotted in 0.5 cm^{-3} bins. The distribution is heavily weighted to less dense clouds. The last bin contains all densities of 10 cm^{-3} or higher.

undercount the number of clouds. The average distance between clouds is dependent only on the inverse cube root of the number of clouds and is thus relatively robust; however, the filling factor is dependent on the total volume of the clouds and thus may be in error by a considerable amount, although it is difficult to imagine that we are missing over 95% of the warm material. Our data are not consistent with the conclusion of Kulkarni & Heiles (1987), based on a number of Hα measurements (see Reynolds 1990a), that the filling factor of the warm gas was 0.5 and the filling factor of the warm, ionized medium (WIM) was 0.11, unless the special environment we are probing has been cleared of dust by the stars themselves.

Considering our selection effects, it is difficult to know just which parameter is a true estimator of the cloud distribution and, pending further modeling, we have chosen to use the fraction of stars in our survey which heat nearby dust as our estimator. In the interest of less involved sentences, we will hereafter refer to this quantity as simply the fraction of stars with dust.

The latitude dependence of the fraction of stars heating dust is tabulated in Table 5 and illustrated in Figure 8 (plus signs). This dependence is fitted reasonably well by a cosecant law (*solid line*) except at the highest latitudes, where the sample size is small. If, however, we break the stars into groups, based on intrinsic luminosity, we find that only the less luminous stars (asterisks in Fig. 8) follow a cosecant law. Not only do a greater fraction of the bright stars heat nearby clouds (diamonds in Fig. 8; cf. Table 3), but the distribution falls of much more slowly with increasing Galactic latitude, perhaps reflecting a more uniform distribution of dust once out of the plane of the Galaxy. It should be cautioned that a much more rigorous approach, including Monte Carlo simulations of the cloud dis-

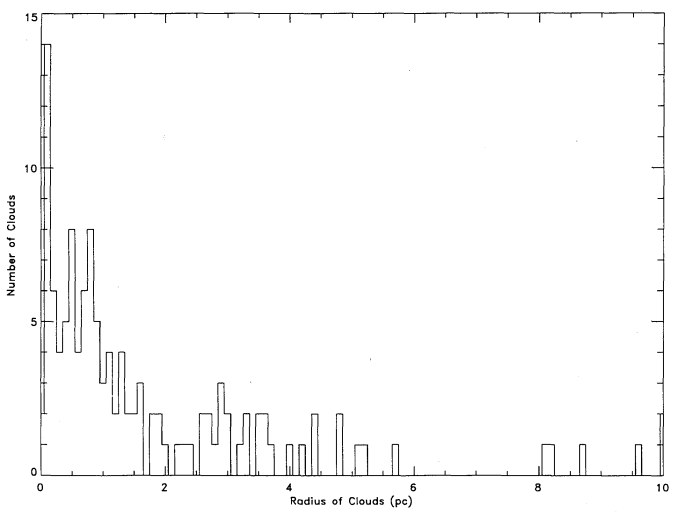

FIG. 6.—A histogram of the number of clouds as a function of radius is plotted. The bin size is 0.1 pc and the last bin contains all clouds of radius 10 pc or greater. Despite the spatial resolution of the instrument, which places a stringent lower limit on the size of a cloud which can be detected (depending on distance), this distribution is heavily peaked to smaller clouds.

TABLE 5

DISTRIBUTION OF CLOUDS WITH LATTITUDE

Latitutde Range	Total Number of Stars	Number of Stars with Dust	Fraction of Stars with Dust
$\|b\| > 50$	79	6	0.076
$40 < \|b\| < 50$	71	4	0.056
$30 < \|b\| < 40$	92	9	0.098
$20 < \|b\| < 30$	203	28	0.138
$10 < \|b\| < 20$	300	59	0.197
Stars of $L_* < 10^{37}$ ergs s^{-1}			
$\|b\| > 50$	67	1	0.015
$40 < \|b\| < 50$	62	4	0.065
$30 < \|b\| < 40$	74	5	0.068
$20 < \|b\| < 30$	164	16	0.098
$10 < \|b\| < 20$	183	26	0.142
Stars of $L_* < 10^{37}$ ergs s^{-1}			
$\|b\| > 50$	12	5	0.417
$40 < \|b\| < 50$	9	0	0
$30 < \|b\| < 40$	18	4	0.222
$20 < \|b\| < 30$	39	12	0.308
$10 < \|b\| < 20$	117	33	0.282

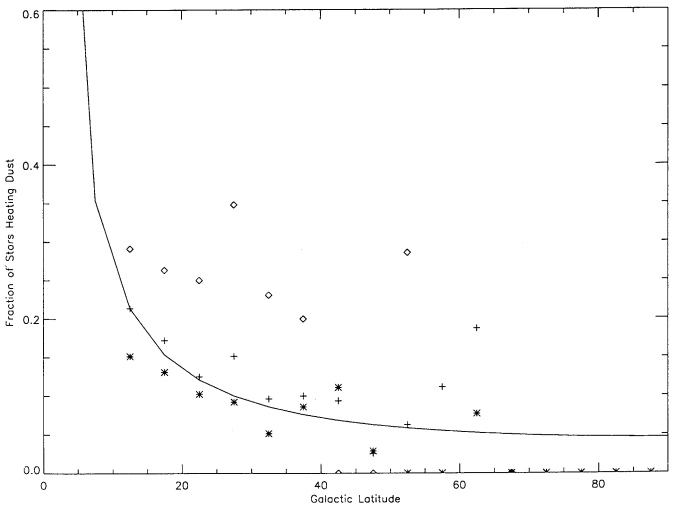

FIG. 8.—The fraction of stars heating nearby dust clouds is plotted as a function of latitude (*plus signs*). The distribution is fitted reasonably well by a cosecant law (*solid line*). We have divided the stars into two groups based on whether their luminosity was less than or greater than 10^{37} ergs s^{-1} and plotted the latitude dependence of the clouds around each group of stars as asterisks and diamonds, respectively. Although the clouds around the less luminous stars (which lie largely in the Galactic plane) still are consistent with a cosecant law, the clouds around the brighter stars appear to follow a much flatter distribution, albeit with poorer statistics, perhaps indicating a more uniform distribution of dust away from the plane.

tributions, will be necessary to ensure that our results are not simply due to selection effects.

The z dependence of the clouds is listed in Table 6 and plotted in Figure 9. The luminosity effects completely mask the relation with height above the Galactic plane for the entire sample, as the fraction of intrinsically bright stars increases

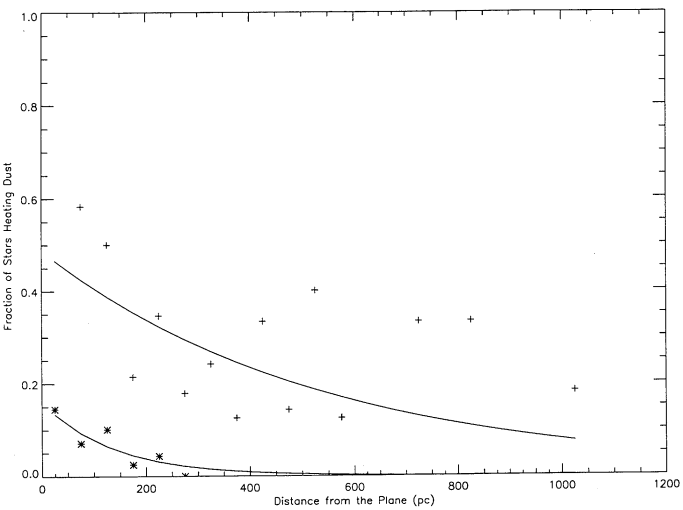

FIG. 9.—The z dependence of the fraction of stars with clouds is plotted for stars with a luminosity less than 10^{37} ergs s^{-1} (*asterisks*) and for those with a greater luminosity (*plus signs*). The two groups follow different distributions and the best-fit (arbitrarily weighting each point by the square root of the number of stars in that bin) exponential distributions to each (*solid lines*) have scale heights of 140 and 540 pc, respectively. This may reflect two populations of dust, one in the plane of the Galaxy (where the cooler stars in our survey tend to lie) and another with a more extended distribution. We detect several clouds at distances of more than 1 kpc from the Galactic plane, more than would be expected even with a scale height of 500 pc from the dust.

TABLE 6

DISTRIBUTION OF CLOUDS WITH HEIGHT ABOVE PLANE

Height above Plane	Total Number of Stars	Number of Stars with Dust	Fraction of Stars Dust
$z < 100$ pc	384	46	0.120
100 pc $< z <$ 200 pc	163	23	0.141
200 pc $< z <$ 300 pc	86	15	0.174
300 pc $< z <$ 400 pc	47	8	0.170
400 pc $< z <$ 500 pc	18	5	0.278
500 pc $< z <$ 1000 pc	36	7	0.194
1000 pc $< z$	11	2	0.182
Stars of $L_* < 10^{37}$ ergs s^{-1}			
$z < 100$ pc	370	39	0.105
100 pc $< z <$ 200 pc	129	10	0.078
200 pc $< z <$ 300 pc	32	1	0.031
300 pc $< z <$ 400 pc	10	0	0.000
400 pc $< z <$ 500 pc	2	1	0.500
500 pc $< z <$ 1000 pc	7	1	0.143
1000 pc $< z$	0	0	
Stars of $L_* > 10^{37}$ ergs s^{-1}			
$z < 100$ pc	14	7	0.500
100 pc $< z <$ 200 pc	34	13	0.382
200 pc $< z <$ 300 pc	54	14	0.259
300 pc $< z <$ 400 pc	37	8	0.216
400 pc $< z <$ 500 pc	16	4	0.250
500 pc $< z <$ 1000 pc	29	6	0.207
1000 pc $< z$	11	2	0.182

with distance, and we have plotted only the fraction of stars with dust for the two luminosity subdivisions in the figure. Aside from the normalization, we find exponential scale heights of 540 pc for the fraction of luminous stars with dust and 140 pc for the less luminous stars, consistent with the idea of two different distributions being sampled by the different stars. These values are comparable to the scale heights of 100–500 pc found from surveys of H I (Lockman, Hobbs, & Shull 1986) and cold cirrus (Burton et al. 1986). There are, however, significantly more clouds far from the plane than would be expected from even a 500 pc scale height, perhaps due to radiation pressure from Galactic plane stars (Franco et al. 1991).

It is difficult to compare these results directly with other studies of the distribution of interstellar matter, either from observations of the gas, namely H I (e.g., Heiles 1976; Burstein & Heiles 1978) and CO (e.g., Sanders, Scoville, & Solomon 1985), or from observations of the dust (e.g., Knude 1979; Feitzinger & Stuwe 1986), because of the very different method and selection effects involved. It is not obvious that the different methods will even select the same population of clouds; the giant molecular clouds (GMCs) of Sanders et al. are obviously a very different population from our sample. We are probing the environment near a number of luminous stars where the dust, and presumably the gas, will be heated by the radiation field of the star and we have tentatively identified our clouds as part of the WIM of McKee & Ostriker (1977), which will be essentially undetectable by, at least, radio observations. Conversely the other methods probe the general ISM and tend to be more sensitive to the cold, neutral medium (CNM).

On the other hand, the low densities in our clouds are similar to the 0.02 cm^{-3} for the average cloud of Knude (1981) from *uvbyβ* photometry of A and F stars. Knude also found a lower limit of 0.7 pc for his distribution of cloud sizes which he hypothesized as either a selection effect or a true lower limit

below which clouds evaporated rapidly. Many of our clouds are, in fact, smaller than this value even though the environment near the luminous stars of our survey is likely to be harsher than the region probed by Knude and hence it seems likely that the lower limit was indeed a selection effect.

Feitzinger & Stuwe (1986), using a complete and uniform set of dark clouds, derived the number density of dark clouds, presumably representing the CNM, to be 8×10^{-5} pc^{-3} within 250 pc of the Sun dropping to 10^{-5} pc^{-3} within 500 pc^{-3} (and to 10^{-6} pc^{-3} within 1000 pc). We obtain a value of 2×10^{-5} pc^{-3} within 200 pc of the Sun for our diffuse clouds, perhaps indicating that the warm, diffuse clouds we sample are less numerous than the colder variety. Again, we will have to examine our selection effects carefully before drawing firm conclusions.

3.2. *Gas Densities*

Probably one of the most important and secure results in this work is the low density around our program stars. We have calculated the density in a series of concentric circles around each of the 745 stars assuming that all the emission above the background at 60 μm is due to thermal emission from dust uniformly distributed around the star, with optical constants from Draine & Lee (1984). An associated error for each point was calculated using the rms deviations of the background in the respective plate, and a weighted average over all the stars was derived (Fig. 10). (It is important to realize that what we call the density is, strictly, not the actual density but is instead an upper limit, including the effects of cool cirrus spatially distant from the star.) The density we derive around each star depends on both the amount of emission nearby and on the strength of the stellar radiation field while the σ's of the density depend on the rms error of the appropriate plate (essentially the same for all the plates), and on the stellar luminosity. Thus the errors will be least near the brightest stars, and the average density will be dominated by the densities near those stars. Most of the contribution to this average comes from two stars (ζ Oph and Spica) for which there is enough

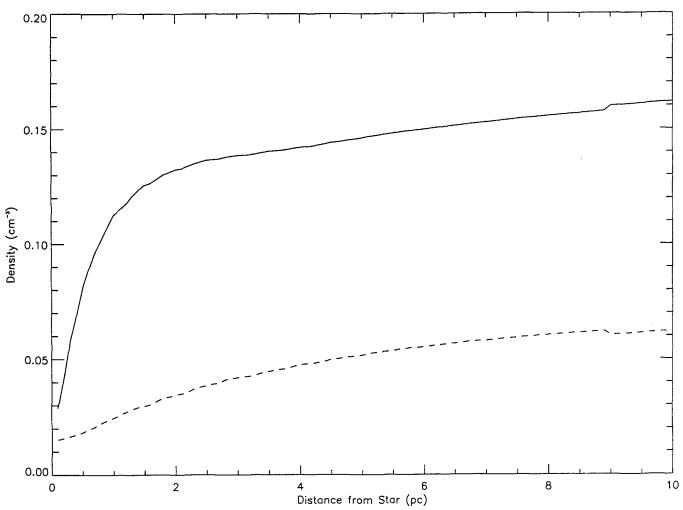

FIG. 10.—The upper limits on the density (using the 60 μm data) near each of the stars have been weighted by the appropriate error bars and summed to yield an average upper limit on the density as a function of distance from the star (*solid line*). This density is heavily weighted by two stars (ζ Oph and Spica), both of which have nearby dust clouds, and if we exclude them, we find a much lower average upper limit of 0.05 cm^{-3} (*dashed line*).

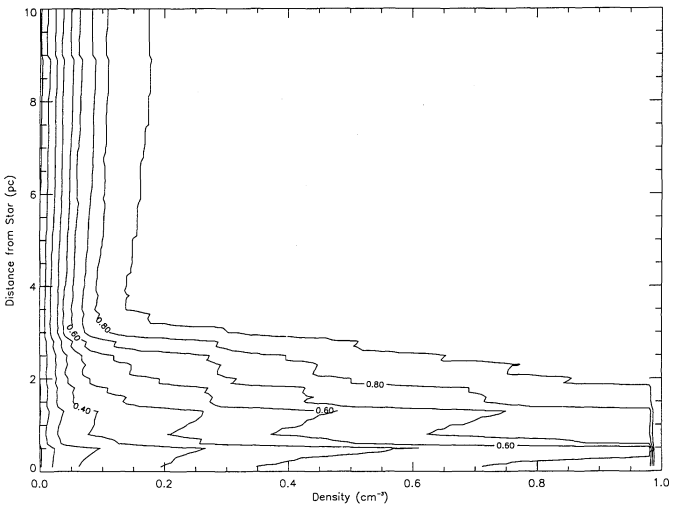

FIG. 11.—Another view of the low densities near the stars in our survey is to show the fraction of stars with densities below the given value. The change in the slope of the contours is caused by our including only stars for which the heat input into the dust exceeds the interstellar value and thus, as we probe farther away from the star, only the most luminous stars—which have better upper limits—are included. At 5 pc from the star, we see that the upper limit on the gas density is less than 0.05 cm^{-3} for about 50% of the stars and less than 0.1 cm^{-3} for about 80% of the stars (including those stars with dust clouds detected nearby).

emission at 60 μm combined with a strong enough stellar radiation field that they dominate the density and, if we exclude these two stars, the upper limit on the density drops from about 0.12 cm^{-3} to 0.05 cm^{-3} (*dashed line*).

Another view of this information is presented in Figure 11 where we have plotted the fraction of stars with a density lower than the abscissa in a volume of radius given by the ordinate; for example, the density of the matter within 6 pc of the central star is less than 0.1 cm^{-3} for 80% of the stars. The shape of the contours in the figure are an artifact of our processing; as the distance from the star increases, we only use those stars for which the stellar radiation field is greater than the ISRF. Thus, at large distances from the central star, we are probing only intrinsically bright stars which will, as discussed above, have more restrictive limits on the amount of nearby dust. If we were to consider only those bright stars, the contours in Figure 11 would be even more restrictive near the star, emphasizing the paucity of dust in our survey.

The exact value of the density is independent on several of our assumptions. The albedo in our model is near 0.5, as given by Draine & Lee (1984). There is, however, evidence that the grains are actually much blacker in the far-ultraviolet (Murthy, Henry, & Holberg 1991; Hurwitz, Bowyer, & Martin 1991) which would drive the densities to even lower values. It has become clear from many studies (see Desert, Boulanger, & Puget 1990 for a summary and references) that a significant part of the 60 μm emission arises from transient heating of small grains, which comprise only a small part of the entire dust population by mass. The Draine & Lee (1984) model does not include this emission and thus the actual density should again be lower. We have also assumed that there is no contribution to the heating from photons below 912 Å, perhaps not true for the low densities found in this work. On the other hand, we have ignored extinction by whatever material is between the star and the point under consideration which would lower the radiation field and thus the heating at that

point, increasing the derived density. Finally, the derived gas density depends on the assumed value of the gas-to-dust ratio. We have used a constant ratio of 5.8×10^{21} atoms cm^{-3} mag^{-1} Bohlin et al. 1978); however, there are strong indications that this value, in fact, varies by at least a factor of 4 in different directions (Burstein & Heiles 1978) and may vary even more near the luminous stars in our study.

A related issue is the amount of stellar energy which escapes the immediate vicinity of the star and contributes to the ionization and energetics of the gas in our Galaxy. The total amount of energy emitted in the *IRAS* bands by all of the dust clouds is 3.7×10^{36} ergs s^{-1} which is 10^{-4} of the total stellar emission. Assuming that about 50% of the total output from the dust is emitted in the *IRAS* bands (Desert et al. 1990), less than 1% of the stellar luminosity is reprocessed near the star, in accord with many other studies of the redistribution of stellar photons. These results are not affected even if we use all of the emissions near the star (Fig. 12), rather than just that part in the clouds identified.

Similar conclusions have been drawn by both Leisawitz & Hauser (1988), who have found, from a study of several OB clusters, that less than 10% of the stellar flux is absorbed within 50 pc of the stars after the stars have moved away from their prenatal molecular clouds, and by Reynolds (1990b) from the high ionization in the local ISM (within 100 pc of the Sun). There are not enough nearby sources to maintain this ionization and therefore UV radiation from O and B stars in the Galactic plane must be reaching the solar neighborhood, implying that there must be paths of low optical depth over that distance.

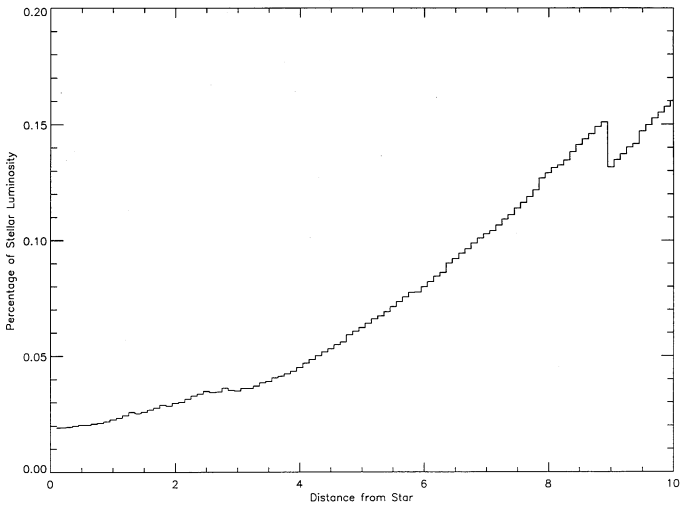

FIG. 12.—The emission within a series of circles around the central star is plotted as function of the radius of the circle as a percentage of the total stellar luminosity. Even within 10 pc of the star, much less than 1% of the stellar flux is emitted within the *IRAS* bands.

4. SUMMARY

We have detected 123 clouds (Table 2) around 106 of a sample of 745 stars for a number fraction of 0.14 ± 0.05. These clouds are similar in properties (Table 4) to those clouds which make up the WIM of McKee & Ostriker (1977) and may form a subsample of that group. If we ignore selection effects, important as they may be in this work, we obtain an average intercloud separation of 46 pc and a volume filling factor of 0.006, much lower than the 0.23 in the McKee-Ostriker theory. There is very little material around the stars except for the clouds, and we place upper limits of abut 0.05 cm^{-3} on the average gas density, which is weighted heavily by the emission near the brightest stars in our survey. We note that this implies that the density of any smooth component of the ISM must be less than this value and that most of the matter must be in the form of discrete clouds, either the diffuse clouds we sample or cold, dark clouds. As a corollary, most of the stellar ionizing flux escapes the neighborhood of the stars into the ISM as a whole.

The latitude dependence of the clouds is fitted reasonably well by a cosecant distribution, except at high galactic latitudes. If one restricts the sample to only the most luminous stars, the falloff with increasing latitude is much less, perhaps reflecting a more uniform distribution of dust once out of the Galactic disk. If we divide our sample into two groups based on luminosity, we find exponential scale heights of 140 and 540 pc for the less luminous and more luminous stars, respectively, again perhaps reflecting differing distributions of dust. We have also found significant numbers of clouds at quite large distances from the Galactic plane.

If our tentative identification of these clouds with the WIM is correct, studying their distribution will yield important clues to the nature of the ISM. We plan to perform Monte Carlo simulations to further understand our observed distribution and the selection effects inherent in our method. We are also studying the individual clouds to study the effects of stellar processing on the dust grains. With the wide range in the radiation fields in our survey, both in intensity and in hardness, we hope to be able to pin down the variations in the properties of the dust as a function of radiation processing and thereby place strong constraints on the physical nature of the dust.

We are grateful to M. Werner, C. Allen, J. Wofford, R. Kimble, C. Mullis, and M. Earl for their contributions to this project. We thank F. Verter and the referee, A. N. Witt, for pertinent comments on the manuscript. Some of this work was done while J. M. was a NRC/NAS Resident Research Associate at NASA/GSFC and this work was supported through NAG-51282. H. J. W. is grateful to the Johns Hopkins University for a visiting fellowship and her work, while at NASA/Ames Research Center, was funded through the SETI Institute under cooperative agreement NCC 2-407. The Bright Star Catalog, SKYMAP, and the *IRAS* Skyflux plates were provided by the National Space Science Data Center and several IDL programs were obtained from the IDL Users Astronomy Library at NASA/GSFC.

REFERENCES

Bohlin, R. C., Savage, B. D., & Drake, J. F. 1978, ApJ, 224, 132
Boulanger, F., Falgarone, E., Puget, J. L., & Helou, G. 1990, ApJ, 364, 136
Boulanger, F., & Perault, M. 1988, ApJ, 330, 964.
Bruhweiler, F. C., & Vidal-Madjar, A. 1987, in Exploring the Universe with the *IUE* Satellite, ed. Y. Kondo (Dordrecht: Reidel), 467
Burstein, D., & Heiles, C. 1978, ApJ, 225, 40
Burton, W. B., Walker, H. J., Deul, E. R., & Jorgenleen, A. W. W. 1986, in Light on Dark Matter, ed. F. P. Israel (Dordrecht: Reidel), 357
de Vries, C. P. 1985, A&A, 150, L15
Desert, F. X., Boulanger, F., & Puget, J. L. 1990, A&A, 237, 214
Draine, B. T., & Lee, H. M. 1984, ApJ, 285, 89
Feitzinger, J. V., & Stuwe, J. A. 1986, ApJ, 305, 534

Franco, J., Ferrini, F., Ferrara, A., & Barsella, B. 1991, ApJ, 366, 443
Gottlieb, D. M. 1978, ApJS, 38, 287
Heiles, C. 1975, A&AS, 20, 37
———. 1976, ApJ, 204, 379
Hoffleit, D. 1982, The Bright Star Catalog (4th rev. ed.; New Haven: Yale Univ. Obs.)
Hurwitz, M., Bowyer, S., & Martin, C. 1991, ApJ, 372, 167
IRAS Explanatory Supplement. 1986, ed. C. A. Beichman, G. Neugebauer, H. J. Habing, P. E. Clegg, & T. Chester (Washington: GPO)
Knude, J. 1979, A&A, 77, 198
———. 1981, A&A, 98, 74
Kulkarni, S. R., & Heiles, C. 1987, in Interstellar Processes, ed. D. J. Hollenbach & H. A. Thronson, Jr. (Dordrecht: Reidel), 87
Kurucz, R. 1979, ApJS, 40, 1
Leisawitz, D., & Hauser, M. G. 1988, ApJ, 332, 954
Lockman, F. J., Hobbs, L. M., & Shull, J. M. 1986, ApJ, 301, 380
Low, F. J., et al. 1984, ApJ, 278, L19
McKee, C. F., & Ostriker, J. P. 1977, ApJ, 218, 148
Murthy, J., Henry, R. C., & Holberg, J. B. 1991, ApJ, 383, 198
Reynolds, R. J. 1990a, IAU Symp. 139, The Galactic and Extragalactic Background Radiation, ed. S. Bowyer & C. Leinert (Dordrecht: Kluwer), 157
Reynolds, R. J. 1990b, ApJ, 345, 811
Sanders, D. B., Scoville, N. Z., & Solomon, P. M. 1985, ApJ, 289, 373
Van Buren, D. 1989, ApJ, 338, 147
Van Buren, D., & McCray, R. 1988, ApJ, 329, L93
Zombeck, M. V. 1982, Handbook of Space Astronomy and Astrophysics (Cambridge: Cambridge Univ. Press)